Telomere length profiles in primary human peritoneal mesothelial cells are consistent with senescence

Melisa Lopez-Anton[a,†], András Rudolf[b,†], Duncan M. Baird[c], Laureline Roger[c], Rhiannon E. Robinson[c], Janusz Witowski[b], Donald J. Fraser[a,d,‡] and Timothy Bowen[a,d,‡,*]

[a]Wales Kidney Research Unit, Division of Infection and Immunity, School of Medicine, College of Biomedical and Life Sciences, Cardiff University, Heath Park, Cardiff CF14 4XN UK

[b]Department of Pathophysiology, Poznan University of Medical Sciences, Poznan, Poland

[c]Division of Cancer and Genetics, School of Medicine, College of Biomedical and Life Sciences, Cardiff University, Heath Park, Cardiff CF14 4XN UK

[d]Cardiff Institute of Tissue Engineering and Repair, Cardiff University, Museum Place, Cardiff CF10 3BG UK

[†]ML-A and AR contributed equally

[‡]DJF and TB contributed equally

*Corresponding author:
Timothy Bowen, Wales Kidney Research Unit, School of Medicine, College of Biomedical and Life Sciences, Cardiff University, Heath Park, Cardiff CF14 4XN, UK
Tel.: +44-29-2074-8389; fax: +44-29-2074-8470; e-mail: bowent@cf.ac.uk

E-mails: ML-A, LopezAntonM@cf.ac.uk; AR, arudolf@umed.poznan.pl; DMB, bairddm@cf.ac.uk; LR, rogerl@cf.ac.uk; RER, jonesr47@cf.ac.uk; JW, jwitow@ump.edu.pl; DJF, fraserdj@cf.ac.uk; TB, bowent@cf.ac.uk

Field Code Changed

Field Code Changed

Running title: Premature mesothelial cell senescence

ABSTRACT

Mesothelial cell (MC) senescence contributes to malignancy and tissue fibrosis. The role of telomere erosion in MC senescence remains controversial, with evidence for both telomere-dependent and telomere-independent mechanisms reported. Single telomere length analysis revealed considerable telomere length heterogeneity in freshly isolated human peritoneal MCs, reflecting a heterogeneous proliferative history and providing high-resolution evidence for telomere-dependent senescence. By contrast the attenuated replicative lifespan, lack of telomere erosion and induction of p16 expression in *in vitro*-aged cells was consistent with stress-induced senescence. Given the potential pathophysiological impact of senescence in mesothelial tissues, high-resolution MC telomere length analysis may provide clinically useful information.

Key words: mesothelium, premature senescence, single telomere length analysis

Formatted: English (United Kingdom)

The mesothelium originates from the embryonic mesoderm surrounding the embryonic coelom and is a significant source of mesenchymal cells for generation of heart, lung, gut, liver and fat (1,2). Adult mesothelial cells (MCs) form a monolayer covering the serosal cavities, uniquely co-express mesenchymal and epithelial markers, and share some properties with vascular endothelium. MC functions include defensive barrier formation, secretion of surface-active lubricant and regulation of inflammation. In peritoneal dialysis therapy, human peritoneal mesothelial cells (HPMCs) form the barrier across which fluid and solute transport take place.

Acquisition by MCs of a senescence-associated secretory phenotype results in increased adherence, angiogenic potential, migration, proliferation, and/or progression in ovarian (3,4), colorectal and pancreatic (5), and mesothelial (6) cancers. In addition, HPMC senescence is accelerated by elevated concentrations of glucose, the main component of solutions used in peritoneal dialysis treatment (7). Therefore understanding MC senescence mechanisms has clinical utility.

Cellular senescence may be triggered by telomere erosion and/or environmental cues. HPMC senescence has been observed *in vitro* after 6 - 10 population doublings (PDs) (8) and mechanisms for both telomere-dependent and telomere-independent HPMC senescence have been reported (9). However, in this work telomeres were sized by quantitative (q)PCR (10-12), which has limited sensitivity and reproducibility that result in systematic bias (13). Furthermore, while this technology estimates telomere repeat content, it does not provide information on telomere length distributions.

To definitively investigate the relationship between telomere length and MC senescence, we used single telomere length analysis (STELA) (14) to analyse XpYp

telomere lengths in early passage and *in vitro*-aged HPMCs. STELA is a high-resolution single molecule approach to determine telomere length with the unique ability to detect telomeres in length ranges that trigger replicative senescence (14,15) or the extreme telomere shortening observed during a telomere-driven crisis (16).

HPMCs were isolated from omentum samples from six different donors and underwent 7.8 - 13.0 PDs (mean 9.3 ± 2.3 PDs) before entering senescence as defined by extensive SA-β-Gal staining, distorted cell morphology, cessation of growth and EdU incorporation, as well as increased IL-6 release and p16 expression (Fig. 1A-D). These PDs represented a shorter replicative lifespan than observed in cell types undergoing telomere-dependent replicative senescence (17) indicating that HPMCs exhibit an extensive replicative history *in vivo* prior to explant. Alternatively, but not necessarily mutually exclusively, these cells may be sensitive to sub-optimal culture conditions and undergo stress-induced senescence in culture.

Additional senescence markers were analysed by RT-qPCR (Figs 1E-K). Increased telomerase reverse transcriptase mRNA was detected in senescent (C_t = 29.12 ± 0.25) compared to young HPMCs (C_t = 29.35 ± 0.31) (Fig. 1K). Conversely, previous telomeric repeat amplification protocol data showed decreased senescent HPMC telomerase activity, and an inverse relationship between telomerase activity and telomere length (10). These data indicate that, irrespective of telomerase expression variation during culture, telomere shortening as a function of MC division in culture might be reduced or insignificant (18).

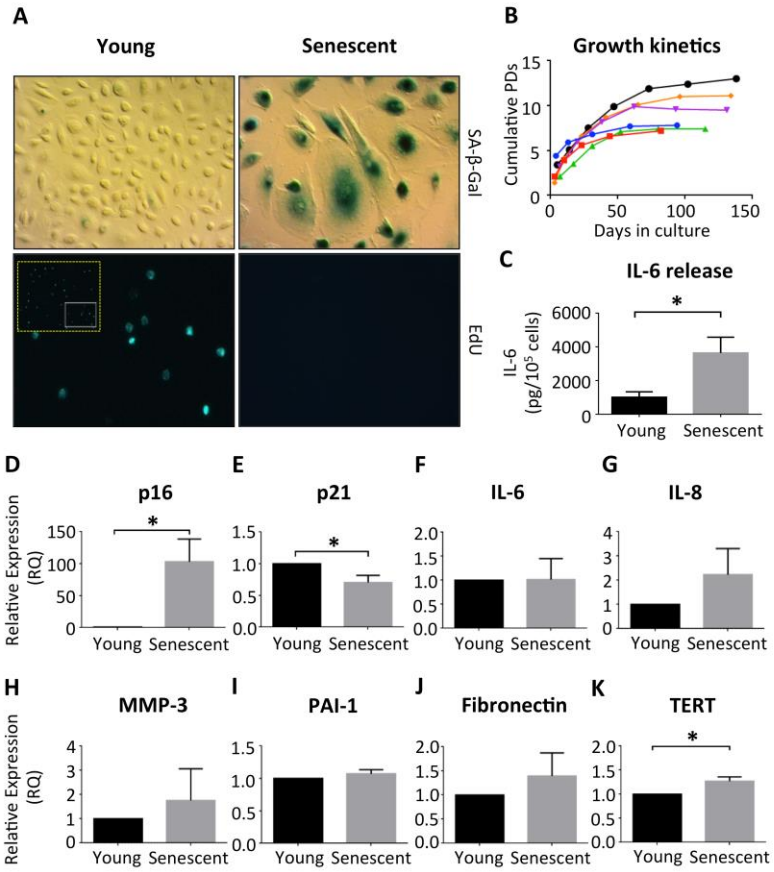

Fig. 1. Analysis of young and senescent primary HPMC populations cultured *in vitro*. **(A)** SA-β-Gal staining and EdU incorporation. **(B)** Cumulative population doublings (PDs) over days in tissue culture (n=6). **(C)** ELISA analysis of IL-6 secretion (n=6). **(D-K)** RT-qPCR detection of cellular senescence markers (n=6): **(D)** p16, **(E)** p21, **(F)** IL-6, **(G)** IL-8, (H) MMP-3, **(I)** PAI-1, **(J)** fibronectin, **(K)** TERT. Where appropriate, data from paired Student's *t*-test analysis are shown: *, $p<0.05$.

STELA of young and senescent HPMCs revealed broadly similar XpYp telomere profiles with pronounced length heterogeneity (Fig. 2A,B). Previously we used STELA to characterise telomere dynamics in primary fibroblast cultures and found a mean telomere length of 5.17 kb in senescent cells (14). Here, STELA analysis showed that both freshly-isolated and *in vitro* senescent HPMCs exhibit an extensive and heterogeneous proliferative history, with a significant proportion of cells displaying telomeres within the length range associated with telomere-dependent senescence (Fig. 2A,B). Indeed, the mean XpYp telomere lengths for young (5.1 ± 2.7 kb) and senescent (5.1 ± 2.6 kb) HPMCs (range of 442 bp - 16.140 kb) varied little, and were consistent with that observed in senescent fibroblast cultures (Fig. 2C).

Previous qPCR data showed significantly increased telomere length in HPMC senescence (10). Consistent with these observations, two of our six senescent populations exhibited increased mean telomere length, which reached statistical significance for one population. We speculate that, if the majority of cells exhibit replicative senescence at the point of explant, serial passage of this culture might lead to preferential loss of cells with shorter telomere length distributions, resulting in an apparent increase in telomere length. However, other situations can be envisaged in which the replicative kinetics might exert a modifying influence on the observed telomere dynamics, within a background of largely senescent cells. For example, oxidative stress is considered to modulate telomere erosion, either directly via telomeric mutation (19) or indirectly by altering the replicative kinetics of cells within the culture (20). Future studies will allow the dissection of the relative contributions of both telomere-driven replicative senescence and stress-induced senescence to the overall HPMC senescence profile.

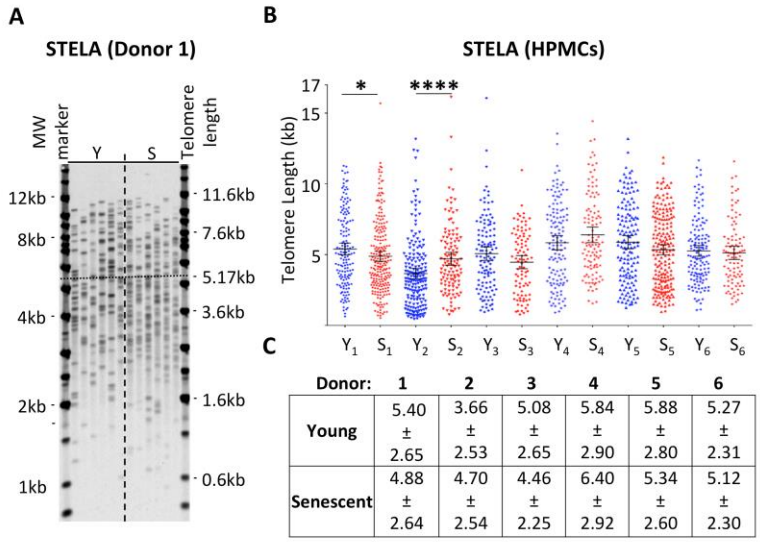

C

Donor:	1	2	3	4	5	6
Young	5.40 ± 2.65	3.66 ± 2.53	5.08 ± 2.65	5.84 ± 2.90	5.88 ± 2.80	5.27 ± 2.31
Senescent	4.88 ± 2.64	4.70 ± 2.54	4.46 ± 2.25	6.40 ± 2.92	5.34 ± 2.60	5.12 ± 2.30

Fig. 2. STELA of young and senescent primary HPMCs. **(A)** Representative Southern analysis of XpYp telomere STELA products. The mean senescent fibroblast telomere length of 5.17 kb is shown by a horizontal dotted line (14). **(B)** Graphical distribution of STELA XpYp telomere lengths (kb) from six different donors are shown for young (Y, red) and senescent (S, blue) cells. Population doublings: S_1, 7.8; S_2, 7.2; S_3, 7.4; S_4, 9.5; S_5, 11.1 and S_6, 13.0. Paired Mann-Whitney non-parametric statistical analysis was performed and mean values ± SEM are shown: *, $p<0.05$; ****, $p<0.0001$. **(C)** Group-specific mean values ± SD.

In summary, we have identified a surprising heterogeneity in primary HPMC telomere length with STELA, a method we have recently used to predict clinical outcome in multiple tumour types including both chronic lymphocytic leukaemia and breast cancer (21,22). Accurate detection of MC telomere lengths by STELA will allow screening for telomere-dependent senescence in patient samples. Given the potential pathophysiological implications for the occurrence of senescent cells in these tissues, we consider that high-resolution telomere length analysis has the potential to provide clinically relevant information in this context.

Conflict of interests

The authors declare no conflict of interests.

Author Contributions

M.L-A., A.R., L.R. and R.E.R. performed the research and analysed the data. D.M.B., J.W., D.J.F. and T.B. designed the research and analysed the data. M.L-A., D.J.F. and T.B. wrote the manuscript.

Funding sources

This work was supported by the European Training and Research in Peritoneal Dialysis (EuTRiPD) Programme, a project funded by the European Union within the Marie Curie Scheme (287813).

Acknowledgements

The Wales Kidney Research Unit is funded by Health and Care Research Wales. M.L-A. and A.R. are supported by the European Training and Research in Peritoneal Dialysis (EuTRiPD) Programme.

Appendix A. Supplementary data

Supplementary data associated with this article can be found, in the online version, at .

References

1. Chau YY, Bandiera R, Serrels A, et al. Visceral and subcutaneous fat have different origins and evidence supports a mesothelial source. *Nat Cell Biol.* 2014;16:367-375.

2. Mutsaers SE. The mesothelial cell. *Int J Biochem Cell Biol.* 2004;36:9-16.

3. Ksiazek K, Mikula-Pietrasik J, Korybalska K, Dworacki G, Jorres A, Witowski J. Senescent peritoneal mesothelial cells promote ovarian cancer cell adhesion: the role of oxidative stress-induced fibronectin. *Am J Pathol.* 2009;174:1230-1240.

4. Mikuła-Pietrasik J, Sosińska P, Naumowicz E, et al. Senescent peritoneal mesothelium induces a pro-angiogenic phenotype in ovarian cancer cells in vitro and in a mouse xenograft model in vivo. *Clin Exp Metastasis.* 2016; 33:15-27.

5. Mikuła-Pietrasik J, Sosińska P, Maksin K, et al. Colorectal cancer-promoting activity of the senescent peritoneal mesothelium. *Oncotarget.* 2015;6:29178-29195.

6. Canino C, Mori F, Cambria A, et al. SASP mediates chemoresistance and tumor-initiating-activity of mesothelioma cells. *Oncogene.* 2012;31:3148-3163.

7. Ksiazek K, Korybalska K, Jorres A, Witowski J. Accelerated senescence of human peritoneal mesothelial cells exposed to high glucose: the role of TGF-beta1. *Lab Invest.* 2007;87:345-356.

8. Connell ND, Rheinwald JG. Regulation of the cytoskeleton in mesothelial cells: reversible loss of keratin and increase in vimentin during rapid growth in culture. *Cell.* 1983;34:245-253.

9. Ksiazek K. Mesothelial cell: a multifaceted model of aging. *Ageing Res Rev.* 2013;12:595-604.

10. Ksiazek K, Passos JF, Olijslagers S, Saretzki G, Martin-Ruiz C, von Zglinicki T. Premature senescence of mesothelial cells is associated with non-telomeric DNA damage. *Biochem Biophys Res Commun.* 2007;362:707-711.

11. Ksiazek K, Mikula-Pietrasik J, Olijslagers S, Jorres A, von Zglinicki T, Witowski J. Vulnerability to oxidative stress and different patterns of senescence in human peritoneal mesothelial cell strains. *Am J Physiol Regul Integr Comp Physiol.* 2009;296:R374-382.

12. Mikuła-Pietrasik J, Kuczmarska A, Rubis B, et al. Resveratrol delays replicative senescence of human mesothelial cells via mobilization of antioxidative and DNA repair mechanisms. *Free Radic Biol Med.* 1-15 2012;52:2234-2245.

13. Verhulst S, Susser E, Factor-Litvak PR, et al. Commentary: The reliability of telomere length measurements. *Int J Epidemiol.* 2015;44:1683-1686.

14. Baird DM, Rowson J, Wynford-Thomas D, Kipling D. Extensive allelic variation and ultrashort telomeres in senescent human cells. *Nat Genet.* 2003;33:203-207.

15. Britt-Compton B, Rowson J, Locke M, Mackenzie I, Kipling D, Baird DM. Structural stability and chromosome-specific telomere length is governed by cis-acting determinants in humans. *Hum Mol Genet.* 2006;15:725-733.

16. Jones RE, Oh S, Grimstead JW, et al. Escape from telomere-driven crisis is DNA ligase III dependent. *Cell Rep.* 2014;8:1063-1076.

17. Allsopp RC, Vaziri H, Patterson C, et al. Telomere length predicts replicative capacity of human fibroblasts. *Proc Natl Acad Sci U S A.* 1992;89:10114-10118.

18. Bodnar AG, Ouellette M, Frolkis M, et al. Extension of life-span by introduction of telomerase into normal human cells. *Science.* 1998;279:349-352.

19. Saretzki G, von Zglinicki T. Replicative senescence as a model of aging: the role of oxidative stress and telomere shortening - an overview. *Z Gerontol Geriatr.* 1999;32:69-75.

20. Britt-Compton B, Wyllie F, Rowson J et al. Telomere dynamics during replicative senescence are not directly modulated by conditions of oxidative stress in IMR90 fibroblast cells. *Biogerontology* 2009;10:683-693.

21. Lin TT, Norris K, Heppel NH, et al. Telomere dysfunction accurately predicts clinical outcome in chronic lymphocytic leukaemia, even in patients with early stage disease. *Br J Haematol.* 2014;167:214-223.

22. Simpson K, Jones RE, Grimstead JW, Hills R, Pepper C, Baird DM. Telomere fusion threshold identifies a poor prognostic subset of breast cancer patients. *Mol Oncol.* 2015;9:1186-1193.

23. Livak KJ, Schmittgen TD. Analysis of relative gene expression data using real-time quantitative PCR and the 2(-Delta Delta C(T)) Method. *Methods.* 2001;25:402-408.

Appendix A. Supplementary data

MATERIALS AND METHODS

Cell Culture

HPMCs were obtained from six different omental donors undergoing abdominal surgery, with ethical approval and informed consent for the use of their omentum for research purposes. After trypsin digestion of the tissue, cells were cultured in M199 Medium (Simga-Aldrich, Gillingham, Dorset, UK) supplemented with 10% fetal calf serum, 2 mM L-Glutamine, 100 U/ml penicillin, 100 µg/ml streptomycin and 0.4 µg/ml hydrocortisone at 37°C in a humidified incubator with 5% CO_2. Culture medium was changed every 2-3 days and cells were passaged at ≥ 90% confluence by trypsinization. Cells were cultured in the above medium prior to STELA, ELISA, SA-β-Gal staining and EdU incorporation, but were growth arrested for 24 h before RNA extraction.

Formatted: English (United Kingdom)

Formatted: English (United Kingdom)

Induction of senescence

HPMC senescence followed successive passages of cells at ≥90% confluence from a fixed seeding density of 7,500 cells/cm^2. Cell numbers were defined using a Bürker chamber and population doublings (PDs) were calculated. HPMCs cultured to senescence tolerated between 7.8 and 13.0 PD (9.3 ± 2.3 PD) with comparable growth dynamics. Cells were regarded as senescent when proliferation ceased and SA-β-Gal staining exceeded 70 %.

SA-β-Gal staining

Cells were seeded in 6-well plates, fixed in 2% formaldehyde / 0.2% glutaraldehyde, washed, and incubated in a solution containing 1 mg/ml 5-bromo-4-chloro-3-indolyl-β-D-galactopyranoside, 5 mM potassium ferrocyanide, 5 mM potassium ferricyanide, 150 mM NaCl, 2 mM $MgCl_2$ and 40 mM citric acid, pH 6.0, for 16 h at 37°C.

EdU incorporation and detection

HPMCs were plated onto glass chamber slides (Lab-Tek, Nunc, Simga-Aldrich) at a density of 15,000 cells/well, then incubated with EdU at a final concentration of 10 μM for 4 hours at 37°C. Cells were fixed with 4% paraformaldehyde and permeabilized with 0.1% Triton X-100 for 10 min. EdU detection was then performed according to the manufacturer's instructions (Sigma-Aldrich). Images were captured with an Axio Observer D1 inverted microscope (Zeiss, Oberkochen, Germany) and analysed using the AxioVision Rel. 4.6.3 image analysis software (Zeiss).

IL-6 detection

HPMC IL-6 levels were measured using the DuoSet Immunoassay Development Kit (R&D Systems, Oxfordshire, UK) according to the manufacturer's instructions.

RNA and genomic DNA isolation

For RT-qPCR analysis, HPMCs were lysed in TRI reagent (Life Technologies, ThermoFisher Scientific, Renfrew, Paisley, UK) and total RNA was extracted in accordance with the manufacturer's instructions. In parallel, HPMCs were also trypsinized and washed three times with cold PBS for genomic DNA extraction using the Maxwell 16 LEV Blood DNA Kit (Promega, Southampton, Hampshire, UK) protocol

with minor modifications. Briefly, cells were resuspended and lysed using a 1 in 10 solution of proteinase K in lysis buffer for 1 h at 56°C. Cell lysates were transferred to a Maxwell 16 LEV Cartridge Rack (Promega) and genomic DNA eluted in 50 µl of elution buffer according to the manufacturer's recommendations.

Reverse transcription-quantitative polymerase chain reaction (RT-qPCR) analysis

Formatted: French (France)

Reverse transcription was carried out using 1 µg of total RNA and the high capacity cDNA reverse transcription kit (Life Technologies) according to the manufacturer's instructions. The ViiA 7 Real-Time PCR System (Life Technologies) was used for the qPCR step, with the Power SYBR Green PCR master mix (Life Technologies) and forward (F) and reverse (R) primer pairs (sequence orientation 5'-3'): p16-F gcccaacgcaccgaatagtt, p16-R cacgggtcgggtgagagt; p21-F ccatgtggacctgtcactgt, p21-R ggcgtttggagtggtagaaa; IL-6-F cgagcccaccgggaacgaaa, IL-6-R ggaccgaaggcgcttgtggag; IL-8-F tcttggcagccttcctgattt, IL-8-R tttggggtggaaaggtttgg; MMP-3-F tctgaggggagaaatcctga, MMP-3-R ggaagagatggccaaaatga; PAI-1-F tctctgccctcaccaacattc, PAI-1-R cggtcattcccaggttctct; Fibronectin-F ccgaggttttaactgcgaga, Fibronectin-R tcacccactcggtaagtgttc; TERT-F ttccgccaggtgtcctgc, TERT-R gcgcacgctggtggtg; GAPDH-F cctctgacttcaacagcgacac, GAPDH-R tgtcataccaggaaatgagcttga. Target mRNA was normalized to GAPDH and relative changes in gene expression were analysed by the $2^{-\Delta\Delta Ct}$ method (23).

Single telomere length analysis (STELA) (14)

Solubilized genomic DNA was quantified and diluted to 10 ng/µl in 10 mM Tris-HCl, pH 7.5. 10 ng of DNA was additionally diluted to 250 pg/µl together with 1 µM Telorette2 linker and 1 nM Tris-HCl, pH 7.5, in a total volume of 40 µl. Six PCRs per study sample

were performed with 250 pg of DNA, 0.5 µM of the telomere-adjacent and Teltail primers, 75 mM Tris-HCl pH 8.8, 20 mM $(NH_4)_2SO_4$, 0.01% Tween-20, 1.5 mM $MgCl_2$, and 1 U of a 25:1 mixture of Taq (ABGene, Epsom, Surrey, UK) and Pwo polymerase (Roche Molecular Biochemicals, Lewes, East Sussex, UK) in a 10 µl reaction volume. A MJ PTC-225 thermocycler (MJ Research, Watertown, MA, USA) was used and the cycle parameters were: 22 cycles of 94°C for 15 s, 65°C for 30 s and 68°C for 10 min. DNA fragments were resolved by 0.5% Tris-acetate-EDTA agarose gel electrophoresis. Southern hybridization was performed using a random-primed α-^{32}P-labeled (Amersham Biosciences, Little Chalfont, UK) telomere-adjacent probe generated by PCR using XpYp primers together with a probe to detect the 1 kb (Stratagene, Agilent Technologies, Stockport, Cheshire, UK) and 2.5 kb (Bio-Rad, Hemel Hempstead, Hertfordshire, UK) molecular weight marker (14). Hybridized fragments were detected by Molecular Dynamics Storm 860 phosphorimager (Amersham Biosciences). The molecular weights of the DNA fragments were calculated using the Phoretix 1D quantifier (Nonlinear Dynamics, Newcastle-upon-Tyne, Northumberland, UK).

Statistical methodology

Data displayed in the text are presented as mean values ± SD, graphical results are expressed as mean values ± SEM. RT-qPCR data were analysed using the paired Student's *t*-test. STELA XpYp telomere length data were analysed using the Mann-Whitney non-parametric statistical test. GraphPad Prism 6 was used for statistical evaluation.

Formatted: English (United Kingdom)